



# Undrained cyclic behaviour of loess with initial shear stress: A focus on failure mode

Xin Liu<sup>a,b,\*</sup>, Zehua Qin<sup>a</sup>, Jun Yang<sup>c,\*\*</sup>

<sup>a</sup> College of Geological Engineering and Geomatics, Chang'an University, Xi'an, 710064, China

<sup>b</sup> Key Laboratory of Ecological Geology and Disaster Prevention of Ministry of Natural Resources, Xi'an, 710054, Shaanxi, China

<sup>c</sup> Department of Civil Engineering, The University of Hong Kong, Hong Kong

## ARTICLE INFO

### Keywords:

Loess  
Cyclic behaviour  
Failure mode  
Initial shear stress  
Excess pore water pressure

## ABSTRACT

Soils in the field conditions, such as in cut slopes or under embankments, often sustains an initial static shear stress prior to the cyclic loadings. Current knowledge on the undrained cyclic behaviour with the presence of initial shear stress has been mainly built on sands. Experimental studies for loess that contains adequate information in this respect is lacking. To fill this gap, this paper presents results from a series of undrained cyclic triaxial tests on the reconstituted and intact loess samples, subjected to different initial static shear stresses. It was found that the existence of initial static shear stress has a significant impact on the failure modes of loess. Three failure modes were observed in the loess samples, including the flow failure, the cyclic mobility and the plastic strain accumulation, among which the flow failure in the reconstituted loess sample was more destructive because of its sudden nature. On the basis of the experiments, we propose a chart to facilitate the identification of the failure modes of loess by taking into account the influence of initial stress state and the excess pore water pressure ( $\Delta u$ ). Specifically, the changes of  $\Delta u$  in the first two cycles are used to distinguish the flow failure and other failure modes. The proposed method is further validated using the literature data, showing a satisfactory predictive performance. The outcome of this study provides a guideline that is useful not only for evaluating undrained cyclic behaviour of loess, but also for predicting the failure modes without the need to load samples to failure.

## 1. Introduction

Earthquake induced instability in loess slopes has been shown to cause severe consequences [1,2]. The 1920 Haiyuan, China earthquake generated massive landslides with long runout distances and demonstrated that flow liquefaction can occur in loess leading to heavy casualties (Fig. 1) [3,4]. Researchers have been studying the undrained cyclic behaviour of soils including the failure modes and the ability against liquefaction in the past several decades and have built up an understanding primarily on granular materials such as sand and gravel [5–7].

Cyclic triaxial and cyclic simple shear tests have revealed that the initial stress state plays a key role to affect the failure modes for granular soils and the number of cycles required to liquefaction in an undrained condition [8–10]. Previous studies show that the impacts of initial shear stress can be either beneficial [11,12] or detrimental [13,14], which is

dependent on several factors including the void ratio, fabric, and confining stress level. A consensus was not reached until that Yang and Sze [15] proposed a unified method for characterizing such effects. A new term in their work, referred to as threshold  $\alpha$  (i.e., initial shear stress ratio), has been confirmed useful in evaluating the failure modes of both clean and silty sands [7,16,17]. The  $\alpha$  value is defined as follows:

$$\alpha = \frac{q_s}{2\sigma'_{nc}} \quad (1)$$

where  $q_s$  is the initial static deviatoric shear stress,  $\sigma'_{nc}$  ( $= (\sigma'_{1c} + \sigma'_{3c})/2$ ) is the normal effective stress on the 45° plane in the sample [18]. The above findings significantly promote the evaluation on cyclic response of granular soils for a range of geotechnical structures with initial shear stress, such as foundations and embankments.

Loess is composed primarily of silt and retains unique features of soil fabric, making their undrained cyclic behaviour more complex than

\* Corresponding author. College of Geological Engineering and Geomatics, Chang'an University, Xi'an, 710064, China. [xliu67@chd.edu.cn](mailto:xliu67@chd.edu.cn)

\*\* Corresponding author.

E-mail addresses: [2016906111@chd.edu.cn](mailto:2016906111@chd.edu.cn) (Z. Qin), [junyang@hku.hk](mailto:junyang@hku.hk) (J. Yang).

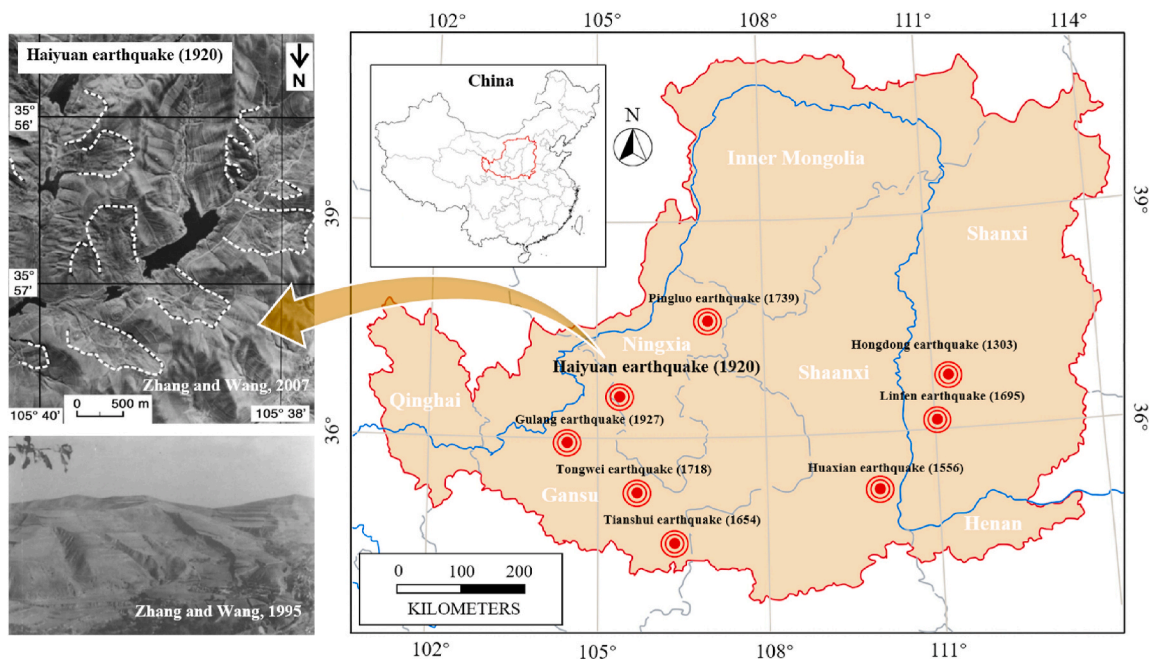


Fig. 1. Major earthquake events in the Chinese Loess Plateau (greater than M7.5).

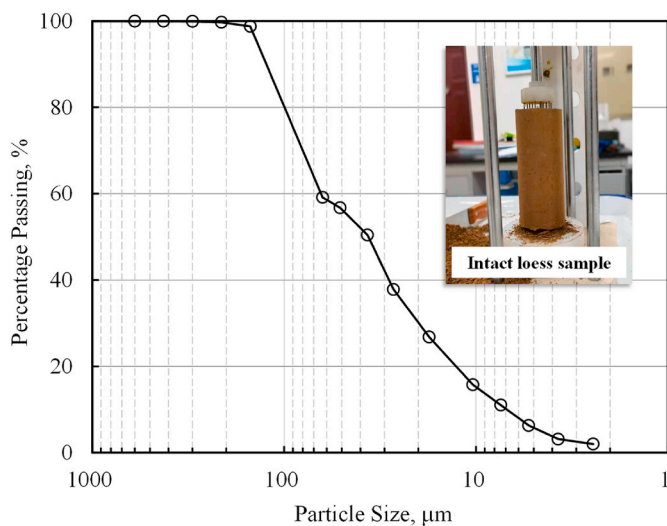


Fig. 2. Particle size distribution curves of tested loess.

Table 1  
Physical properties of tested loess.

Soil Sample	$C_u$	$d_{50}$ ( $\mu\text{m}$ )	$d_{10}$ ( $\mu\text{m}$ )	PL	PI	$G_s$
Loess	9.27	36.43	6.96	19.9	7.0	2.65

Note:  $C_u$ : coefficient of uniformity;  $G_s$ : specific gravity; PL: plastic limit; PI: plasticity index.

granular soils. Although some pioneer works in loess have been conducted by several researchers [18–21], the experimental studies on the undrained cyclic behaviour of loess are rather limited, and the results appear to be controversial. For example, Hyodo et al. [22] performed cyclic triaxial tests on silt prepared by the sedimentation method. They reported that increasing initial shear stress will decrease the liquefaction resistance for a condition with the stress reversal, but it becomes beneficial for that with no stress reversal. These findings are inconsistent with the results by Yang and Sze [15] on quartz sand and Sağlam and

Bakr [23] on saturated silt. In the current literature, compared with the extensive research on granular soils, a lack of comprehensive experimental data impedes a good understanding of the undrained cyclic behaviour in loess. In particular, investigations on the failure modes of loess considering the effect of initial shear stress have not been reported.

To address these concerns, this paper presents experimental results from a series of undrained cyclic triaxial tests on both intact and reconstituted loess samples. The influence of initial shear stress on the failure modes of loess was investigated. On the basis of test results, a chart method was established to evaluate the failure mode for loess, taking into account the changes of excess pore water pressure in the first two cycles and the initial stress state. The outcomes of this study not only show an insight into the undrained cyclic behaviour of loess, but also provide a fundamental basis for future research on possible prewarning of failures in loess under the cyclic loads.

## 2. Experimentation

### 2.1. Test materials and sample preparation

Undisturbed loess samples used in this study were collected from a construction site in Yan'an city, China. Particle size distribution of the tested loess confirmed that the loess can be classified as a sandy silt according to the British Standards (BS 1377–2) (Fig. 2). The basic soil properties are listed in Table 1. The orientations of the intact samples were marked immediately after sampling from the field, and all samples were carefully wrapped with plastic films and sealed with wax to avoid any disturbance or loss of moisture during transportation. The in-situ water content of the loess is about 11.6%, and the initial void ratio is between 0.67 and 0.79 in the depth from 3 m to 4 m. Prior to the cyclic triaxial test, the intact loess samples were carefully trimmed into cylindrical specimens with 39.1 mm in diameter and 80 mm in height. In addition, disturbed loess specimens were reconstituted from the trimmings using the moist tamping method in conjunction with the under-compaction technique. The under-compaction technique is referred to the concept brought by Ladd [24], in which it creates overall more uniform moist-tamped specimen than using layers of equal dry weight and volume [25,26]. As shown in Fig. 3, a target void ratio of 0.775 (similar with the intact loess samples) was achieved by compacting a

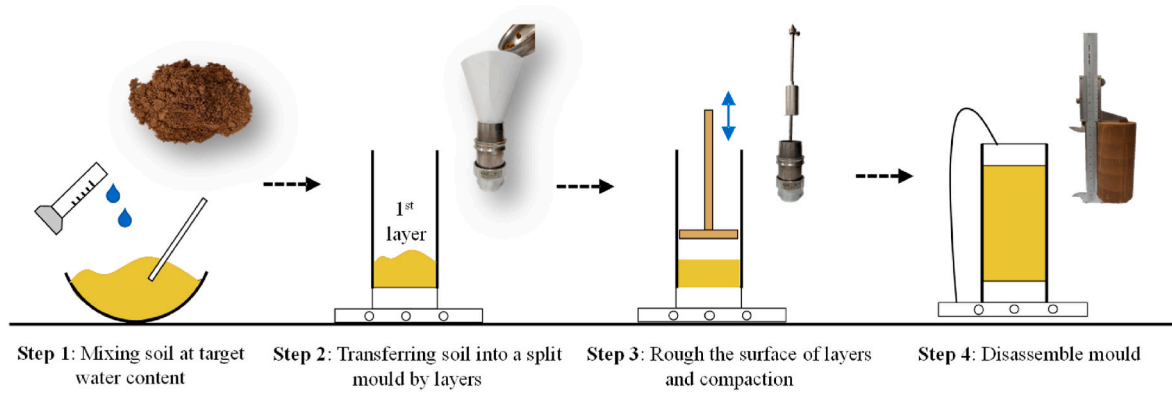


Fig. 3. Schematic illustration of moist tamping method.

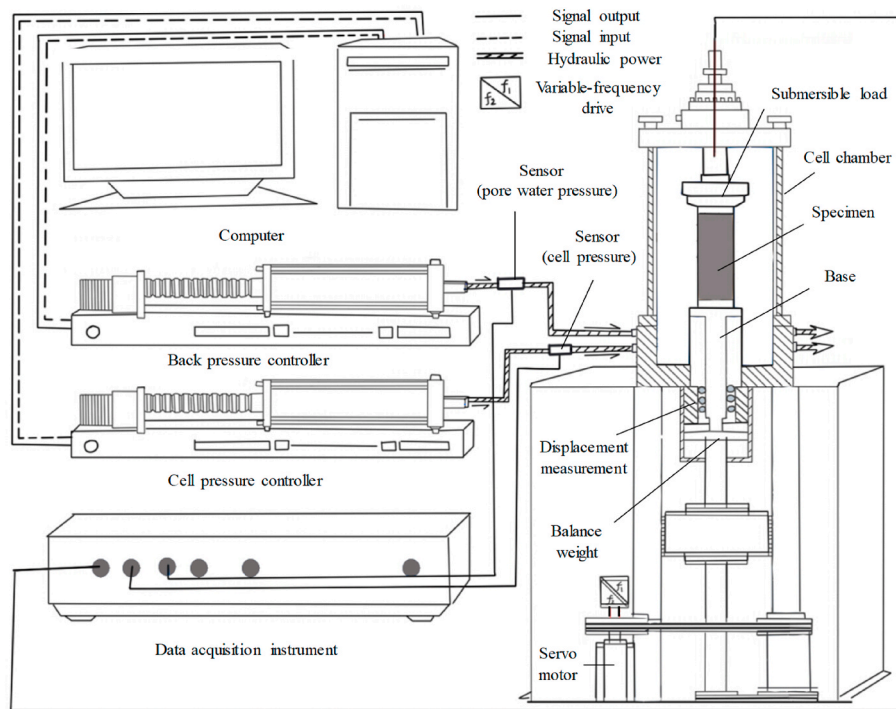


Fig. 4. Schematic illustration of the dynamic triaxial apparatus used in this study.

predetermined mass of wet soil into five layers of equal thickness in a split mould. Here, the loess was prepared with an initial water content of 11.6%, and the degree of under-compaction was varied linearly from the bottom to the top layer, with an under-compaction ratio of 1%.

## 2.2. Test apparatus and test program

After sample preparation, each loess sample was carefully placed in the triaxial chamber, and was subjected to a saturation process. In this study, all specimens were saturated in two stages: initially by flushing the specimen with carbon dioxide and de-aired water, and then by applying a stepwise increased back pressure [27]. To achieve the full saturation state, a Skempton  $B$  value greater than 0.95 was required [28]. All tests were conducted under the stress-controlled mode through an automated cyclic triaxial testing system (Fig. 4), which is capable of performing isotropic and anisotropic consolidation. In the latter case, the specimen was consolidated by controlling the principal effective stresses  $\sigma'_{1c}$  and  $\sigma'_{3c}$  in small increments such that a constant initial shear stress ratio ( $\alpha$ ) was maintained until the desired stress condition was reached.

In this study, the target  $\sigma'_{3c}$  is 100 kPa for all tests. In cases where the initial shear stress is absent,  $\sigma'_{nc}$  is equal to the minor principal consolidation stress ( $\sigma'_{3c}$ ). In each test, cyclic stress ( $q_{cyc}$ ) were applied to the specimen in a sinusoidal waveform at a frequency of 0.1 Hz, which is considered as representative of the typical frequency range of seismically induced loading, and is also to ensure the accurate measure of pore water pressure under cyclic loads [29]. Here, if  $q_{cyc}$  exceeds the initial static shear stress ( $q_s$ ) in magnitude, the loading is known to be with stress reversal; otherwise, it is without reversal. A total of 28 cyclic undrained triaxial tests were conducted on isotropically and anisotropically consolidated loess specimens. A summary of test series is listed in Table 2. Noting that “Re” and “In” denote the reconstituted and intact loess, respectively.

## 3. Test results and discussion

### 3.1. Cyclic failure modes in reconstituted loess

In Figs. 5–7, cyclic responses of the reconstituted loess with different magnitudes of initial shear stress are shown. ‘ $N_f$ ’ in each diagram

**Table 2**  
Summary of test series in this study.

Test	$e_0$	$e_c$	$q_s$ (kPa)	$\alpha$	$q_{cyc}$ (kPa)	Failure mode
Re-1	0.768	0.746	0	0.00	30.8	CM
Re-2	0.757	0.744	0	0.00	24.2	CM
Re-3	0.761	0.747	0	0.00	27.6	CM
Re-4	0.761	0.723	19.2	0.09	41.7	CM
Re-5	0.765	0.727	18.3	0.08	45.1	CM
Re-6	0.770	0.715	17.5	0.08	45.8	CM
Re-7	0.763	0.726	19.2	0.09	47.5	CM
Re-8	0.767	0.717	20.0	0.09	38.3	CM
Re-9	0.770	0.624	94.2	0.32	32.6	FF
Re-10	0.771	0.612	97.5	0.33	25.3	FF
Re-11	0.777	0.601	93.3	0.32	16.7	FF
Re-12	0.773	0.601	91.7	0.31	20.9	FF
In-1	0.762	0.749	0.0	0.00	33.3	CM
In-2	0.787	0.744	0.0	0.00	37.7	CM
In-3	0.717	0.673	0.0	0.00	43.3	CM
In-4	0.722	0.688	0.0	0.00	48.1	CM
In-5	0.750	0.645	65.0	0.25	51.6	CM
In-6	0.741	0.643	61.7	0.24	91.7	CM
In-7	0.787	0.657	68.3	0.25	82.5	CM
In-8	0.671	0.651	67.0	0.25	100.5	CM
In-9	0.703	0.623	90.0	0.31	82.6	PA
In-10	0.758	0.646	91.7	0.31	87.5	PA
In-11	0.711	0.626	92.0	0.32	88.7	PA
In-12	0.694	0.612	92.9	0.32	99.5	PA
In-13	0.779	0.618	95.6	0.32	107.4	PA
In-14	0.711	0.606	215.5	0.52	31.5	PA
In-15	0.720	0.608	220.8	0.52	40.8	PA
In-16	0.711	0.601	219.2	0.52	36.7	PA

Note: CM: Cyclic mobility; FF: Flow failure; PA: Plastic strain accumulation.

denotes the number of cycles at failure. In Fig. 5,  $\alpha$  is zero, indicating no initial shear stress. It is clear to see a complete stress reversal in  $q$ - $p'$  and  $q$ - $\epsilon_a$  diagrams. As the cyclic loading proceeded,  $p'$  decreased gradually towards zero. A transient liquefied state of the specimen, known as initial liquefaction [7,30] was observed, which was followed by a substantial regain of the effective stress and stiffness in the sample. This process was repeated in sequent loading cycles, accompanied by prominent stiffness degradation. In this experiment, the failure of sample took place until unacceptably large axial strain was approached (in the 31st cycle). It is noted that the above undrained failure mode is referred to as 'cyclic mobility', which frequently occur in medium to dense sand specimens under cyclic loads subjected to stress reversal [31, 32]. As shown in Fig. 5(b) and (c), the reconstituted loess sample was failed under extension ( $\epsilon_a$  is less than zero).

In Fig. 6, a positive initial shear stress ( $\alpha = 0.09$ ), being less than the cyclic stress ( $q_{cyc}$ ), was applied on a reconstituted loess sample. The deviatoric stress is non-symmetric about the hydrostatic stress axis in  $q$ - $p'$  diagram. In this case, the cyclic mobility was observed. The axial strain was predominantly accumulated in the compression side of each loading cycle (Fig. 6(b) and (c)). Hence, it is rational that the sample approached failure under the compression state (in the 78th cycles). Furthermore, the cyclic response of a reconstituted loess sample subjected to no stress reversal is presented in Fig. 7. As the cyclic loading proceeded,  $p'$  gradually decreased, while the axial strain increased with the number of cycles. Also worthy of note in this case is that the loess soil behaves very contractively under the normal confining stress of 100 kPa, and the failure of sample occurred in a sudden (in the 89th cycles), triggering of marked deformation in a short period (Fig. 7(c)). Specifically, prior to the failure (within the first 88 cycles), the axial deformation of the sample is about 2%, whereas it increases to nearly 30% after the failure. This abrupt failure style is referred to as flow failure for soils under cyclic loads [15,33–35]. Compared with other types of failures, the flow failure in soils is more destructive in the field due to less prewarning [36], such as the Haiyuan earthquake as shown in Fig. 1.

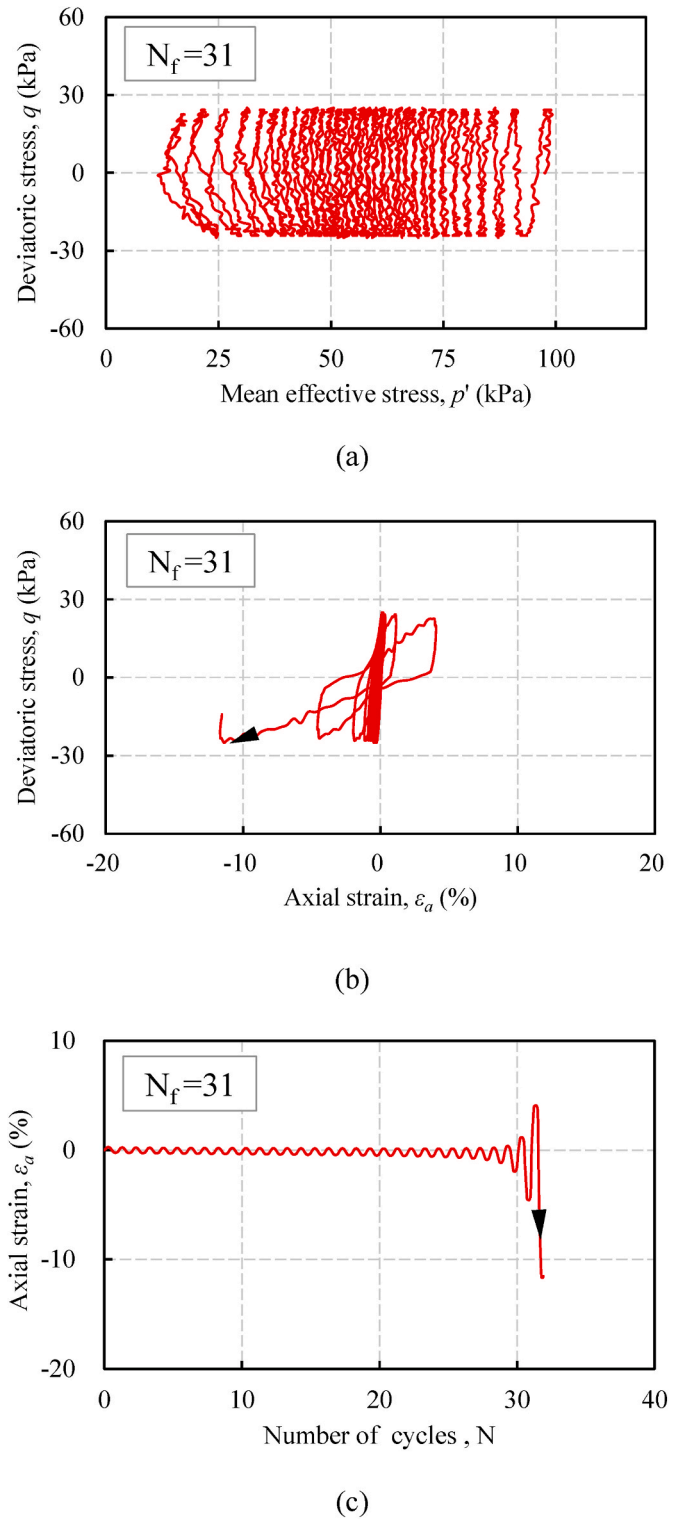


**Fig. 5.** Undrained response of reconstituted loess with complete stress reversal ( $e_c = 0.744$ ,  $\alpha = 0$ ,  $q_s = 0$  kPa,  $q_{cyc} = 24.2$  kPa).

### 3.2. Cyclic failure modes in intact loess

Compared with the reconstituted loess, the intact loess often exhibits higher shear strength, as reported in the literature in terms of higher internal friction angle and peak strength [37]. In this study, experiments were also conducted on the intact loess samples to evaluate whether the initial shear stress influences the cyclic failure modes of the intact loess.

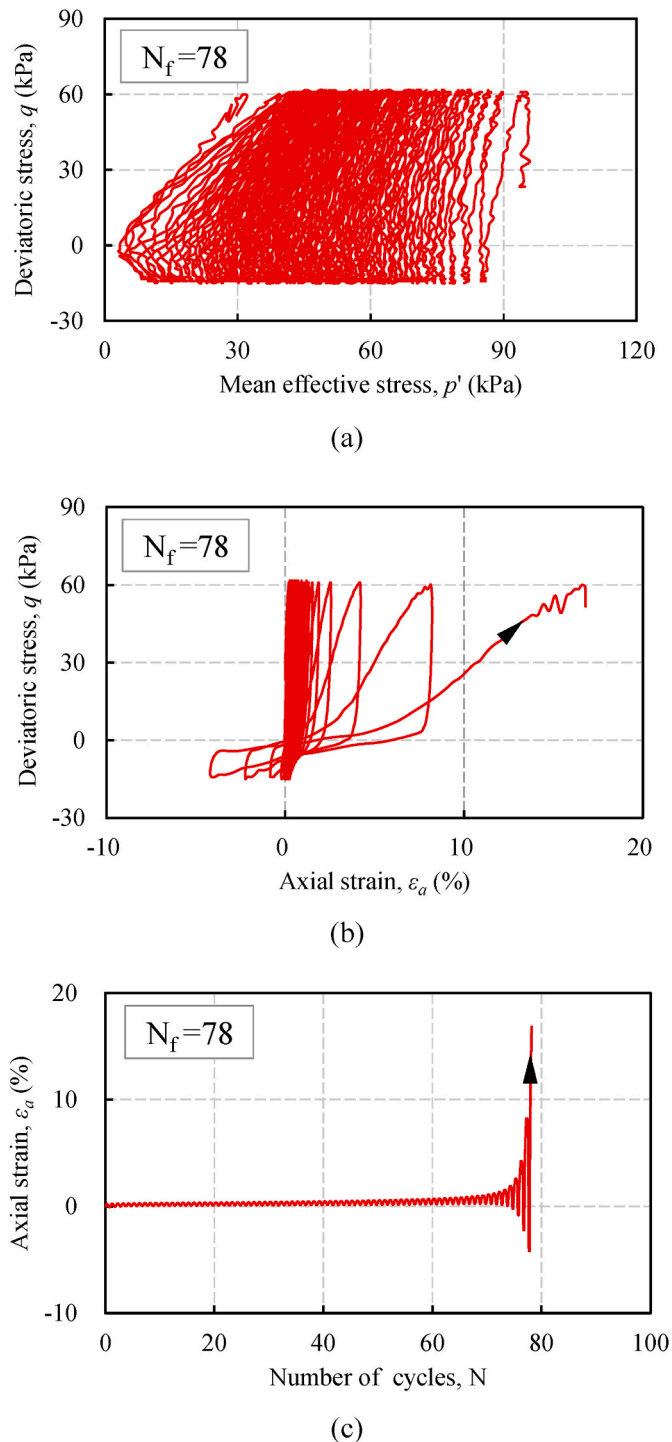


Fig. 6. Undrained response of reconstituted loess with partial stress reversal ( $e_c = 0.717$ ,  $\alpha = 0.09$ ,  $q_s = 20$  kPa,  $q_{cyc} = 38.3$  kPa).

In Fig. 8, the test results of an intact loess sample with no initial shear stress are presented. The cyclic responses are similar with that of the reconstituted loess sample as shown in Fig. 5, and both displayed the behaviour of cyclic mobility. Nevertheless, although the applied cyclic stress ( $q_{cyc} = 33.3$  kPa) is greater on the intact sample than that on the reconstituted one ( $q_{cyc} = 24.2$  kPa), more loading cycles are required for the intact sample to reach failure. This finding is consistent with the expectation that the intact loess has a higher cyclic resistance.

Besides, the test results of intact loess samples with different  $\alpha$  values are presented in Figs. 9 and 10, and they are shown as the conditions of

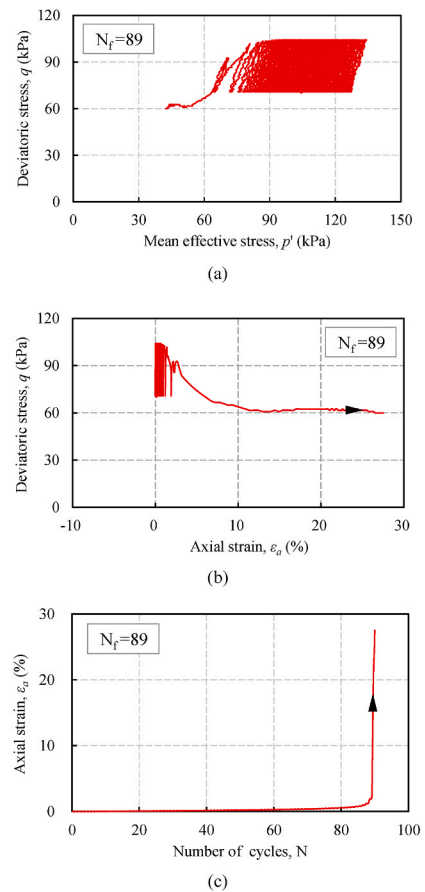


Fig. 7. Undrained response of reconstituted loess with no stress reversal ( $e_c = 0.601$ ,  $\alpha = 0.32$ ,  $q_s = 93.3$  kPa,  $q_{cyc} = 16.7$  kPa).

partial stress reversal and no stress reversal, respectively. In the former case, the cyclic mobility occurred (Fig. 9), which is in general the same failure mode for the reconstituted loess in Fig. 6. An interesting comparison is given in Figs. 7 and 10, where a similar  $\alpha$  value was applied in both the intact and reconstituted samples, representing by the condition of no stress reversal. In Fig. 10 (b) and (c), it is clear that the flow failure as illustrated in Fig. 7 did not occur for the intact loess sample. Rather, the intact sample reached the failure by a progressive accumulation of plastic strain. At end of the test, the failure occurred during compression of the cyclic loading.

From the above observations in Figs. 5–10, one can conclude that the cyclic response of loess is strongly affected by the initial stress state and the applied cyclic load. In particular, when no stress reversal is applied, caution should be exercised about the possibility of flow failure in the reconstituted loess, and it is unlikely occurred in the intact ones.

### 3.3. Excess pore water pressure accumulation

In the undrained cyclic triaxial test, the fluctuations of mean effective stress are associated with the changes of excess pore water pressure ( $\Delta u$ ). Thereby, the above failure modes in the loess samples can also be interpreted by  $\Delta u$ . In Fig. 11, test results from the reconstituted and intact loess samples under zero initial shear stress are compared. Although both cases yielded the behaviour of cyclic mobility, less cycles were required for the reconstituted loess sample to reach the maximum  $\Delta u$ . These findings are consistent with the experiments illustrated in Figs. 5 and 8. Moreover, in Fig. 12,  $\Delta u$  is plotted respectively for the reconstituted and intact loess samples with different magnitudes of initial shear stress. In Fig. 12(a), in particular in the reconstituted sample with no stress reversal,  $\Delta u$  increases gently at the initial loading stage,

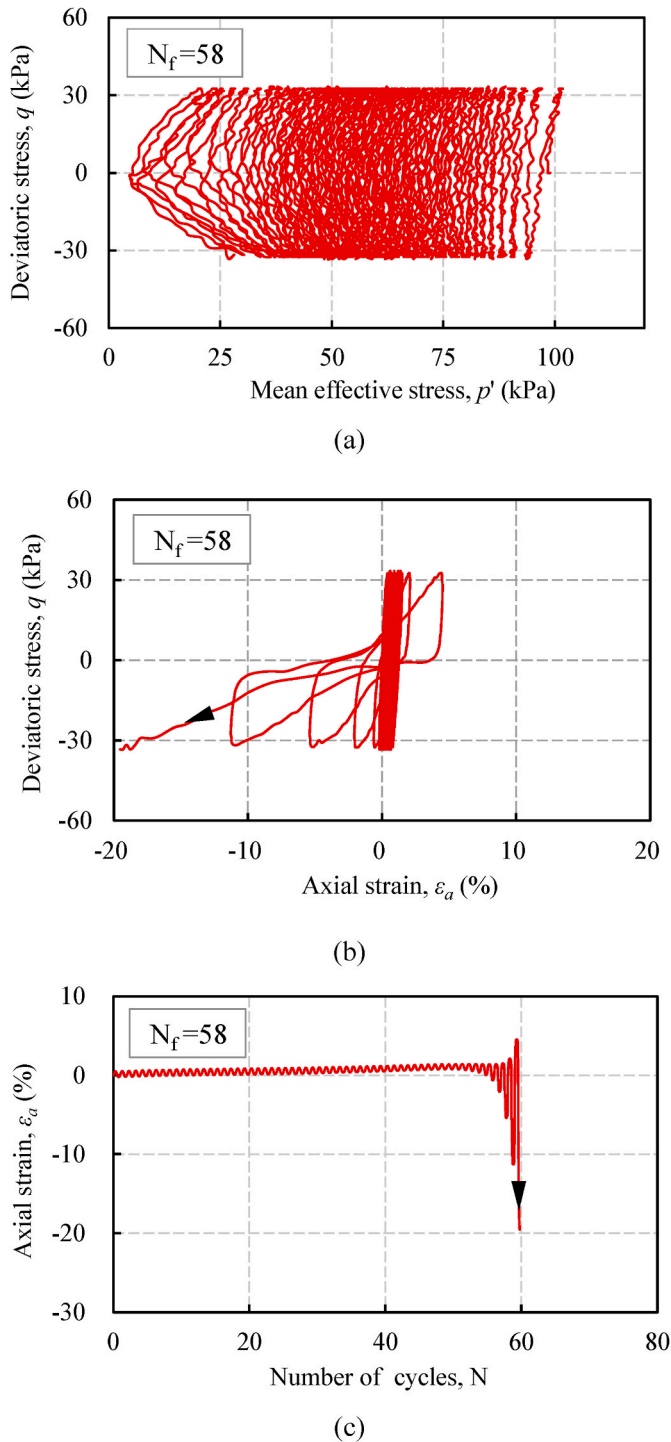


Fig. 8. Undrained response of intact loess with complete stress reversal ( $e_c = 0.749$ ,  $\alpha = 0$ ,  $q_s = 0$  kPa,  $q_{cyc} = 33.3$  kPa).

which is followed by a dramatic rise of  $\Delta u$  in the 89th cycle (point “a”). As shown in Fig. 7, the above trend is also accompanied by a marked decrease in the mean effective stress, and it is referred to as the flow failure. In Fig. 12(b), the excess pore water pressure in the intact loess samples increases gradually, confirming that no flow failure occurred in the intact loess samples. Compared with the case of partial stress reversal, an increasing number of loading cycles were required to reach the maximum  $\Delta u$  in the sample with no stress reversal, and it is referred to as the plastic strain accumulation.

Furthermore, to quantify the changes of  $\Delta u$ , the slope of the line

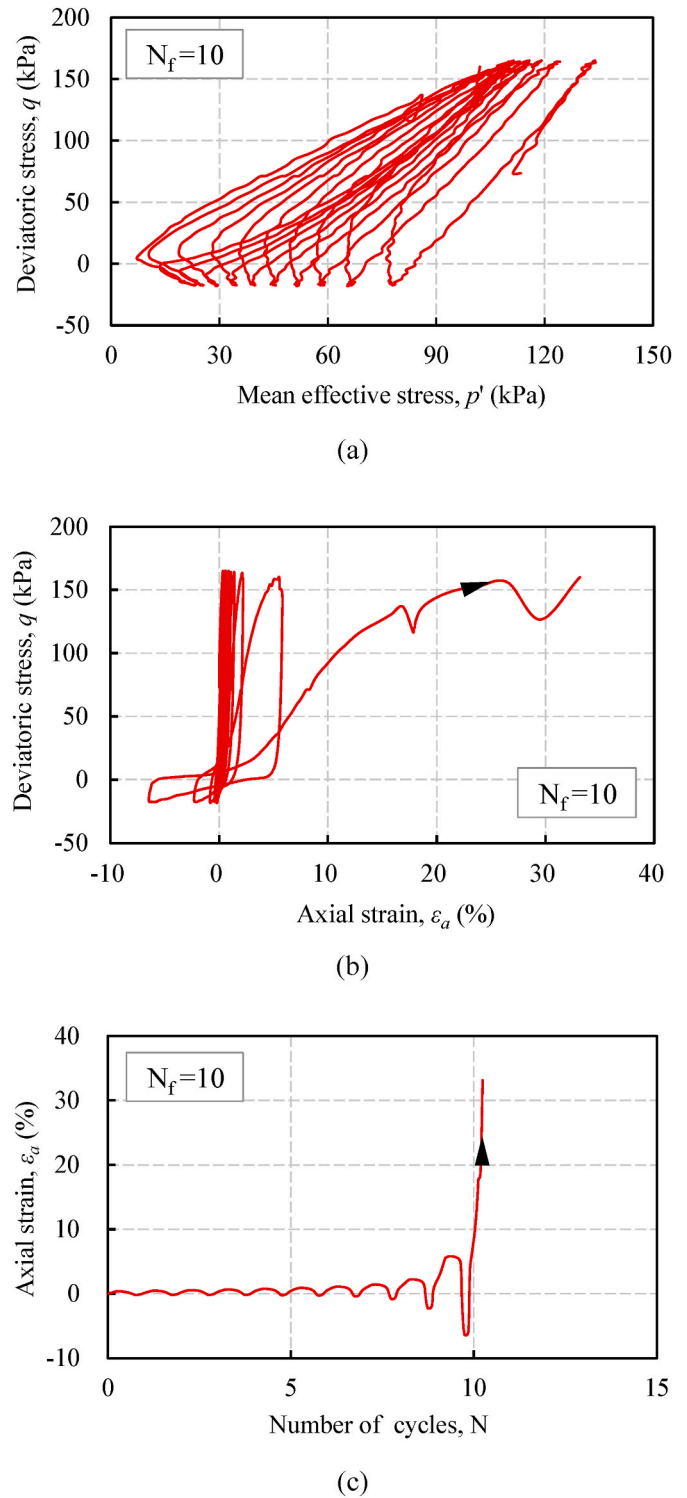
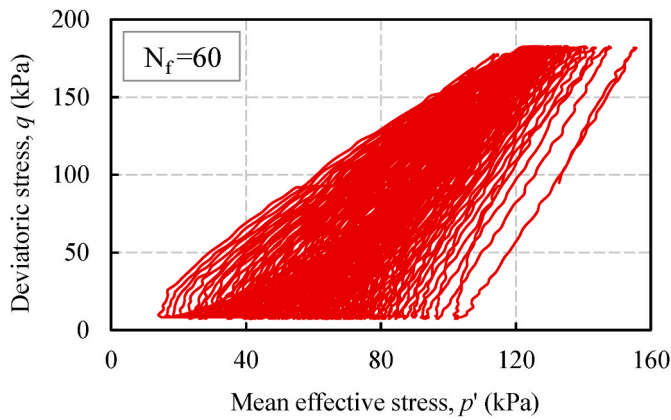


Fig. 9. Undrained response of intact loess with partial stress reversal ( $e_c = 0.643$ ,  $\alpha = 0.24$ ,  $q_s = 61.7$  kPa,  $q_{cyc} = 91.7$  kPa).

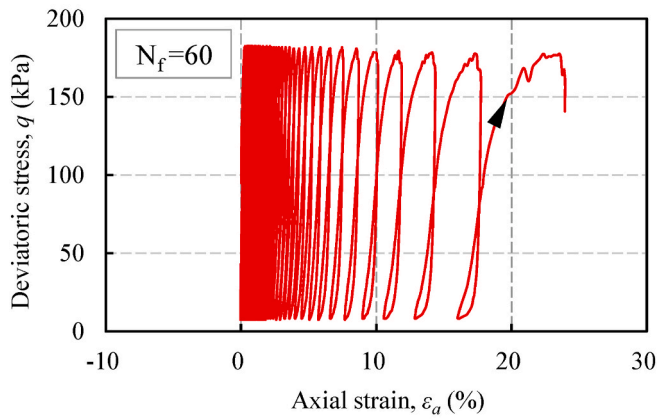
connecting the peaks of two successive cycles, as shown in Fig. 13, is adopted in the following analysis. The slope is denoted as  $K$  (in kPa) in the equation as below.

$$K = \frac{\Delta u_n - \Delta u_{n-1}}{N_n - N_{n-1}} \quad (2)$$

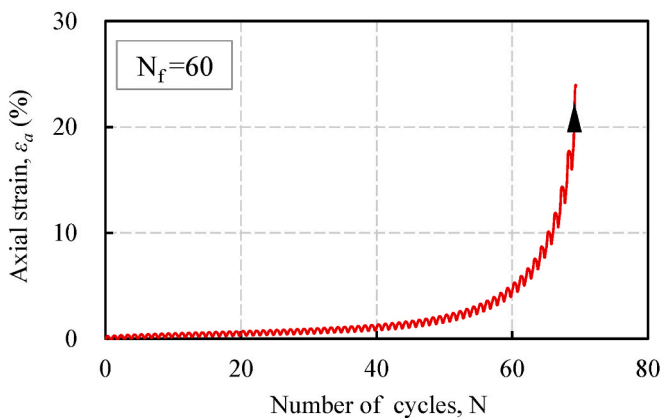
where  $\Delta u_n$  is the peak  $\Delta u$  in the  $n$ th cycle, and  $N$  is the number of cycles. Of particular concern is which cycles are proper for estimating the  $K$



(a)



(b)



(c)

**Fig. 10.** Undrained response of intact loess with no stress reversal ( $e_c = 0.646$ ,  $\alpha = 0.31$ ,  $q_s = 91.7$  kPa,  $q_{cyc} = 87.5$  kPa).

value. To address this concern, Fig. 14 compares the  $K$  values based on  $\Delta u$  in the first two cycles ( $K_{1-2}$ ) with that at failure ( $K_f$ ), for the three failure modes observed. It is worth noting that  $\Delta u$  in the first cycle is critical for determining the number of cycles required to cause failure in sand, as observed by Ni et al. [38] and Oda et al. [39]. Instead of using the  $\Delta u$  in the first cycle, the  $K$  value proposed here characterizes the changes of  $\Delta u$  in successive loading cycles.

In Fig. 14, three sets of  $K$  values are shown in each diagram for different failure modes in loess, including the plastic strain

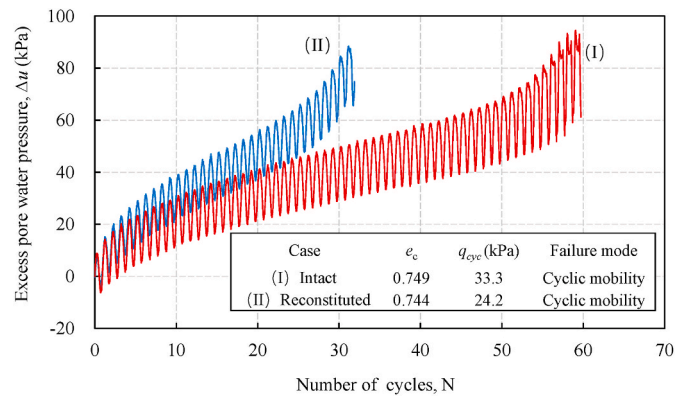
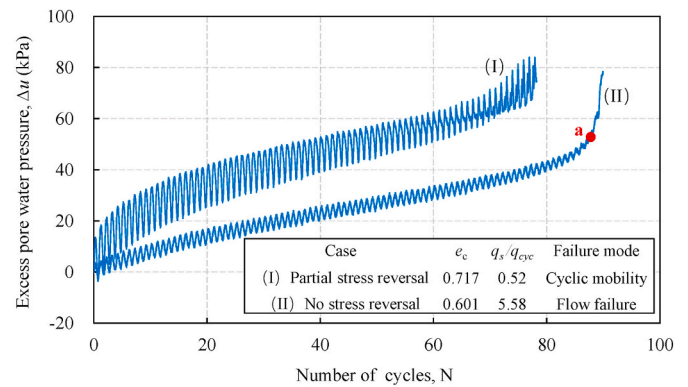
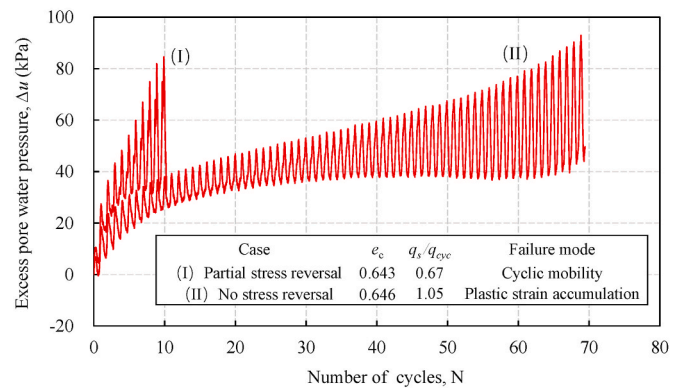


**Fig. 11.** Excess pore water pressure of intact and reconstituted loess without initial shear stress.



(a)



(b)

**Fig. 12.** Excess pore water pressure of intact and reconstituted loess under initial shear stress: (a) reconstituted loess; (b) intact loess.

accumulation (PA), the cyclic mobility (CM) and the flow failure (FF). The results for all tests listed in Table 2 are compiled in this figure. Although the after-consolidation void ratios of loess specimens are slightly different, no clear trend was observed between the  $K$  values and the void ratios, with an implication that the void ratio has no significant impact on the  $K$  values. Besides, two important features are observed: (1) the loess samples exhibiting the flow failure have markedly narrow distributions of  $K$  values than that in other failure modes. In particular, in the FF mode the range between the upper and lower values of  $K_{1-2}$  is smaller than that of  $K_f$ ; (2) compared with  $K_f$ , the average values of  $K_{1-2}$

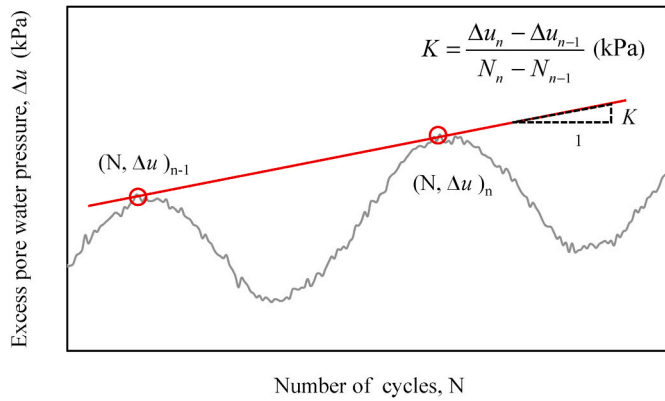


Fig. 13. Definition of  $K$  value in the excess pore water pressure.

in Fig. 14(a) are significantly different. It implies that  $K_{1-2}$  is more sensitive to the failure mode in loess, thereby  $K_{1-2}$  has a potential as an indicator to distinguish the failure modes in loess samples.

3.4. A chart method for identifying failure modes

Given the above evidence, an attempt was made to identify different failure modes of loess in Fig. 15 by establishing a chart using  $q_s/q_{cyc}$  and  $K_{1-2}$ . Here,  $q_{cyc}$  is the applied cyclic stress, and  $q_s$  is the initial static deviatoric shear stress. Besides, the solid symbols were used for the intact loess specimens and the hollow symbols are for the reconstituted ones. When  $q_s/q_{cyc}$  is greater than one, it represents the condition of no stress reversal, accordingly a no-reversal line is plotted in this figure. As shown in Fig. 15(a), when  $K_{1-2}$  is smaller than 1.96, the loess samples displayed the flow failure. When  $K_{1-2}$  is greater than 3.96, it exhibited either the mode of plastic strain accumulation or the cyclic mobility mode. The above findings suggest the existence of a threshold  $K_{th}$  for identifying the mode of flow failure in loess. For other failure modes, they can be distinguished in this diagram by the data with the position against the no-reversal line. For example, when  $K_{1-2}$  is greater than 3.96 and the stress ratio is less than one ( $q_s/q_{cyc} < 1$ ), the cyclic mobility prevailed in the loess samples (indicated by the circles in the diagram). Based on the experimental results, four individual zones can be identified in the chart, as shown in Fig. 15(b). In this study,  $K_{th}$  is found in a range of 1.96–3.96. No data are found in the blank zone, where  $K_{1-2}$  is small and the samples are subjected to the stress reversal.

Note that Fig. 15(a) includes the data from both the reconstituted and intact loess samples. It is worthwhile to further validate the chart using additional experimental data. In doing so, more data are extracted from the experiments reported in the literature and they are re-interpreted and plotted in Fig. 16. Fig. 16(a), (b) and (c) show the results of the Hebei fine sand from Xu et al. [40], the tailing silts from Tan et al. [41], and the fine sand from an earth dam project from Zhang et al. [42], respectively. Moreover, an extra group of data on the reconstituted loess with an addition of 10% fine sand by mass is included in Fig. 16(d). It is very encouraging to note that regardless of different test materials, the proposed method works reasonably well in predicting the failure modes, and  $K_{th}$  value varies with different materials.

The proposed chart is promising in several aspects. First, it confirms that the initial stress state and the excess pore water pressure in initial loading stage in loess are of importance to evaluate the failure mode. For a given  $q_s/q_{cyc}$  that is smaller than one, it is unlikely to observe the flow failure in loess samples. Second, the introduction of a threshold  $K_{th}$  helps predict the different failure modes without the need for loading the sample to failure. Based on the experimental data, it can be suggested that the effective mean to avoid the flow liquefaction in loess is to decrease the  $q_s/q_{cyc}$ . In the meanwhile, the resistance to flow may be improved if the excess pore water pressure in the first cycle is depressed and the  $K_{1-2}$  is greater than  $K_{th}$ .

4. Conclusions

This paper presents experimental results on the undrained cyclic behaviour of loess specimens under different initial stress states. The major conclusions are summarized as follows:

- (1) The loess specimen with the stress reversal exhibited the cyclic mobility. If there is no stress reversal, the reconstituted loess specimen showed the mode of flow failure, while the intact loess specimen showed the mode of plastic strain accumulation. The flow failure in the reconstituted loess sample was more destructive because of its sudden nature. Cautions should be exercised about the possibility of flow failure.
- (2) On the basis of test results, a chart was established to characterize the cyclic failure modes in loess, by considering the changes of the excess pore water pressure in the first two cycles together with the non-stress-reversal line. In particular, a threshold  $K_{th}$  was found for identifying the flow failure in loess.

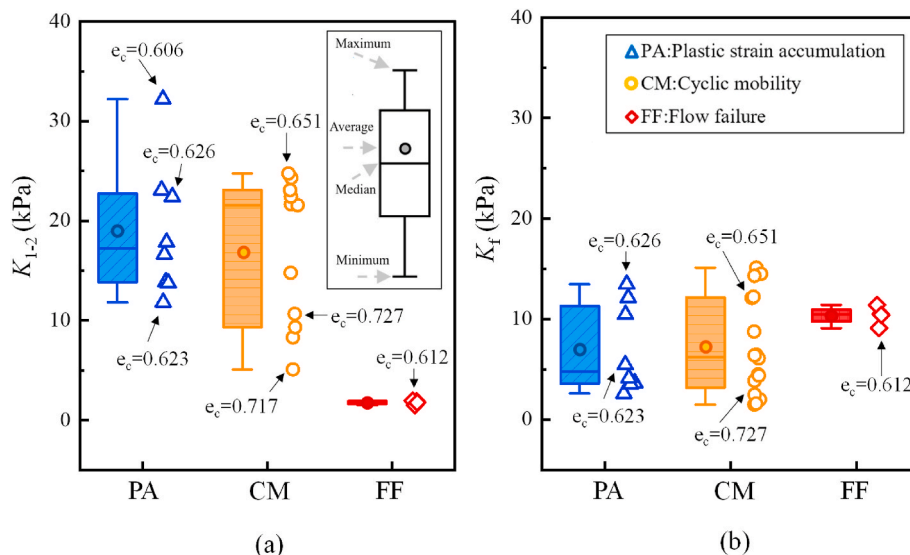
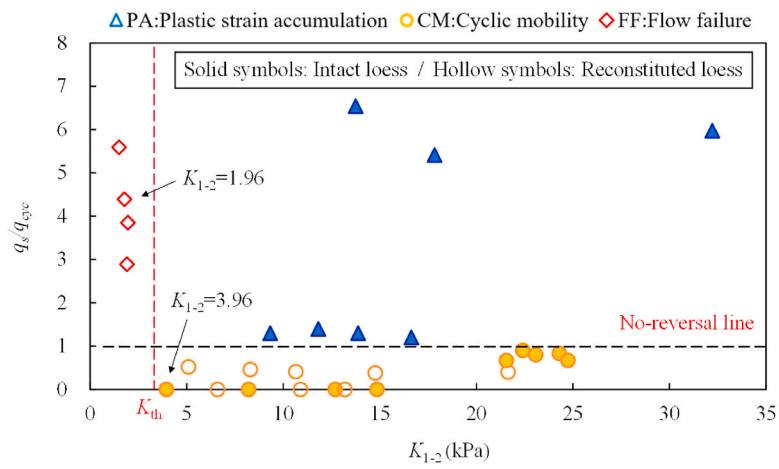
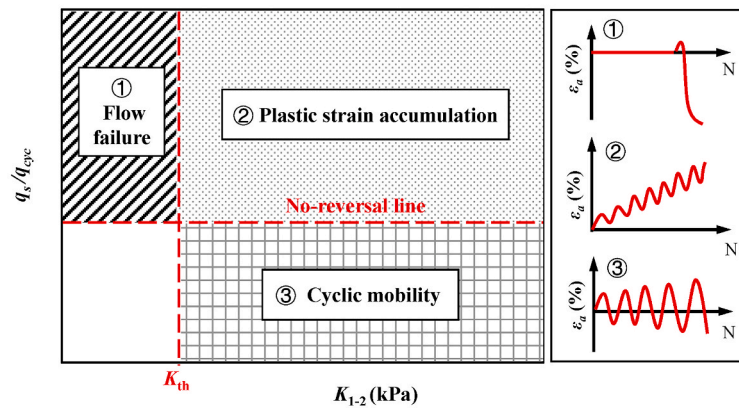


Fig. 14. Box diagram of  $K$  value: (a) at first two cycles; (b) at failure.



(a)



(b)

Fig. 15. Chart method for identifying failure modes.

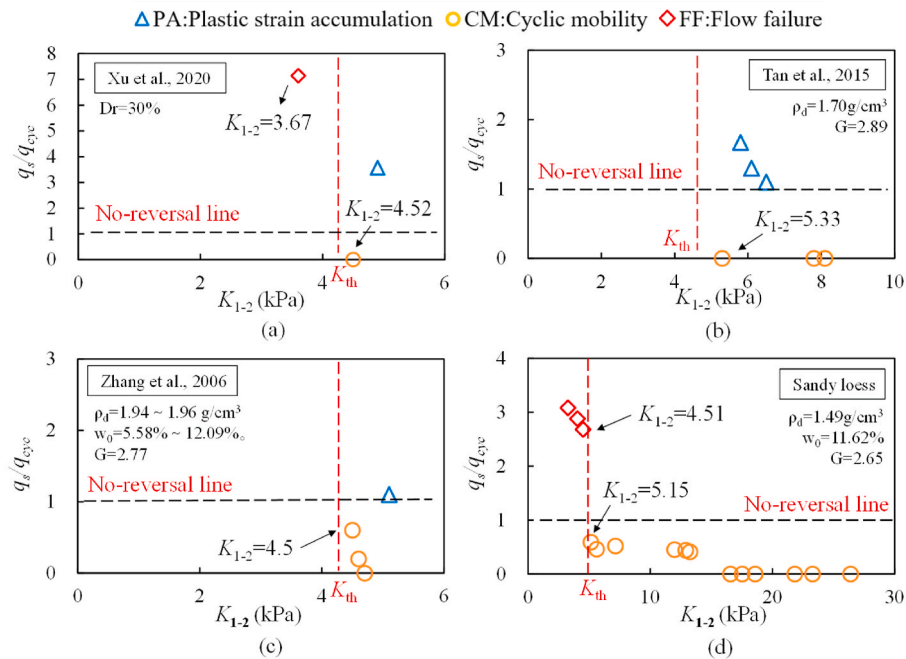


Fig. 16. Validation of the proposed chart against extra experimental data and literature data.

(3) Experimental data from the literature were used to validate the proposed chart method, and a good predictive performance was obtained. The new method is encouraging, because it helps to distinguish the failure modes of loess without the need for loading the sample to failure. Thereby, it provides a fundamental basis for future research on possible prewarning of cyclic failures in loess.

#### Author statement

Conceptualization, Xin Liu; Methodology, Xin Liu and Jun Yang; Investigation, Zehua Qin; Writing-original draft, Xin Liu and Jun Yang; Writing-review and editing, Xin Liu and Zehua Qin; Project administration, Xin Liu; Funding acquisition, Xin Liu.

#### Declaration of competing interest

The authors declare that they have no known competing financial interests or personal relationships that could have appeared to influence the work reported in this paper.

#### Data availability

Data will be made available on request.

#### Acknowledgments

The present study is supported by the National Natural Science Foundation of China (No. 42041006; 41927806), the Natural Science Basic Research Plan in Shaanxi Province of China (No. 2022JQ-251) and the Fundamental Research Funds for the Central Universities through Chang'an University, China (No. 300102263101). These financial supports are gratefully acknowledged.

#### References

- Carey JM, Mcsaveney MJ, Petley DN. Dynamic liquefaction of shear zones in intact loess during simulated earthquake loading. *Landslides* 2017;14(3):789–804.
- Ishihara K, Okusa S, Oyagi N, Ischuk A. Liquefaction-induced flow slide in the collapsible loess deposit in Soviet Tajik. *Soils Found* 1990;30(4):73–89.
- Zhang D, Wang G. Study of the 1920 Haiyuan earthquake-induced landslides in loess (China). *Eng Geol* 2007;94(1–2):76–88.
- Zhang ZZ, Wang LM. Geological disasters in loess areas during the 1920 Haiyuan earthquake, China. *Geojournal* 1995;36(2):269–74.
- Borja R. Conditions for liquefaction instability in fluid-saturated granular soils. *Acta Geotech* 2006;1:211–24.
- Flora A, Lirer S, Silvestri F. Undrained cyclic resistance of undisturbed gravelly soils. *Soil Dynam Earthq Eng* 2012;43(4):366–79.
- Sze HY, Yang J. Failure modes of sand in undrained cyclic loading: impact of sample preparation. *J Geotech Geoenviron Eng* 2014;140(1):152–69.
- Ishihara K. *Soil behaviour in earthquake geotechnics*. Oxford, UK: Oxford Science Publications; 1996.
- Kokusho T. Major advances in liquefaction research by laboratory tests compared with in situ behavior. *Soil Dynam Earthq Eng* 2016;91:3–22.
- Wichtmann T, Triantafyllidis Th. Influence of a cyclic and dynamic loading history on dynamic properties of dry sand, part II: cyclic axial preloading. *Soil Dynam Earthq Eng* 2004;24:789–803.
- Liu Z, Qian J, Yaghoubi M, Xue J. The effects of initial static deviatoric stress on liquefaction and pre-failure deformation characteristics of saturated sand under cyclic loading. *Soil Dynam Earthq Eng* 2021;149:106870.
- Seed HB. *Earthquake-resistant design of earth dams*. Proc., Symp. On Seismic Design of Earth Dams and Caverns, ASCE 1983:41–64.
- Hyodo M, Orense RP, Noda S, Furukawa S, Furui T. Slope failures in residential land on valley fills in Yamamoto town. *Soils Found* 2012;52(5):975–86.
- Yoshimi Y, Oh-Oka H. Influence of degree of shear stress reversal on the liquefaction potential of saturated sand. *Soils Found* 1975;15(3):27–40.
- Yang J, Sze HY. Cyclic strength of sand under sustained shear stress. *J Geotech Geoenviron Eng* 2011;137(12):1275–85.
- Wei X, Yang J. Cyclic behavior and liquefaction resistance of silty sands with presence of initial static shear stress. *Soil Dynam Earthq Eng* 2019;122:274–89.
- Yang J, Liang LB, Chen Y. Instability and liquefaction flow slide of granular soils: the role of initial shear stress. *Acta Geotech* 2022;17(1):65–79.
- Wei X, Yang J. Characterizing the effect of particle size disparity on liquefaction resistance of non-plastic silty sands from a critical state perspective. *Geotechnique* 2021;24(2):1–14.
- Liu X, Miao XQ, Qin ZH, Huang GJ, Lan HX. Shear behavior of loess: the role of drainage condition. *Eng Geol* 2022;309:106835.
- Wang S, Luna R, Zhao H. Cyclic and post-cyclic shear behavior of low-plasticity silt with varying clay content. *Soil Dynam Earthq Eng* 2015;75:112–20.
- Zhang Z, Wang T, Wu S, Tang HM, Xin P, Liang CY. Dynamics stress-strain behavior of Tianshui soils. *Landslides* 2017;14(1):323–35.
- Hyodo M, Hyde AFL, Aramaki N, Nakata Y. Undrained monotonic and cyclic shear behavior of sand under low and high confining stresses. *Soils Found* 2002;42(3):63–76.
- Saglam S, Bakir BS. Cyclic response of saturated silts. *Soil Dynam Earthq Eng* 2014;61–62:164–75.
- Ladd RS. Preparing test specimens using under compaction. *Geotech Test J* 1978;1(1):16–23.
- Liu X, Wang YC, Nam BH. Characterizing undrained shear behavior of loess subjected to K0 loading condition. *Eng Geol* 2022;302:106634.

- [26] Liu X, Wei X, Qin H. Characterizing compressive strength of compacted saline loess subjected to freeze-thaw cycling with wave velocity. *Bull Eng Geol Environ* 2022; 81(4):1–10.
- [27] Yang J, Liu X. Shear wave velocity and stiffness of sand: the role of non-plastic fines. *Geotechnique* 2016;66(6):500–14.
- [28] Zhang N, Liu X, Lan HX. Characterizing saturation state of loess using P-wave velocity. *Eng Geol* 2021;290:106207.
- [29] Hyodo M, Murata H, Yasufuku N, Fujii T. Undrained cyclic shear strength and residual shear strain of saturated sand by cyclic triaxial tests. *Soils Found* 1991;31(3):60–76.
- [30] Pan K, Yang ZX, Cai YQ. Flow liquefaction potential of loose sand: stress path envelope and energy-based evaluation. *Can Geotech J* 2021;58(11):1783–9.
- [31] Andrade JE. A predictive framework for liquefaction instability. *Geotechnique* 2009;59(8):673–82.
- [32] Wang G, Xie Y. Modified bounding surface hypoplasticity model for sands under cyclic loading. *J Eng Mech* 2014;140(1):91–101.
- [33] Pan K, Xu T, Liao D, Yang Z. Failure mechanisms of sand under asymmetrical cyclic loading conditions: experimental observation and constitutive modelling. *Geotechnique* 2020;72(2):162–75.
- [34] Vaid YP, Stedman JD, Sivathayalan S. Confining stress and static shear effects in cyclic liquefaction. *Can Geotech J* 2001;38(3):580–91.
- [35] Kokusho T, Hazarika H, Ishizawa T, Ishibashi S, Ogo K. Unprecedented liquefaction flow of gentle slopes containing non-plastic fines. *Pro Ins Civ Eng Foren Eng* 2022; 175(2):31–8.
- [36] Seed HB, Lee KL. Liquefaction of saturated sands during cyclic loading. *J Geotech Geoenviron Eng* 1966;92(6):105–34.
- [37] Xu L, Coop MR, Zhang M, Wang G. The mechanics of a saturated silty loess and implications for landslides. *Eng Geol* 2018;236:29–42.
- [38] Ni XQ, Zhang Z, Ye B, Zhang S. Unique relation between pore water pressure generated at the first loading cycle and liquefaction resistance. *Eng Geol* 2022;296: 106476.
- [39] Oda M, Kawamoto K, Suzuki K, Fujimori H, Sato M. Microstructural interpretation on reliquefaction of saturated granular soils under cyclic loading. *J Geotech Geoenviron Eng* 2001;127(5):416–23.
- [40] Xu CS, Feng CQ, Du XL, Zhang XL. Study on liquefaction mechanism of saturated sand considering stress redistribution. *Eng Geol* 2020;264:105302.
- [41] Tan F, Rao XB, Huang B, Wang ZB, Xu YY. Experimental study on dynamic characteristics of saturated tailings silt. *China Earthq Eng J* 2015;37(3):772–7 (in Chinese).
- [42] Zhang R, He CR, Fei WP, Gao MZ. Effect of consolidation stress ratio on dynamic strength and dynamic pore water pressure of soil. *Chin J Geotech Eng* 2006;28(1): 101–5 (in Chinese).